Astrophysics Group
Cavendish Laboratory

Characterization of the primordial non-Gaussianity using wavelets

Andrés Curto

Overview

- Forecasts by different inflationary scenarios on the CMB anisotropies:
  - Common shapes of primordial non-Gaussianity
- Contaminants on the primordial NG:
  - “Point sources”
  - “Integrated Sachs-Wolfe and lensing interplay”
- How do we measure the weak signals produced by the NG?
  - Wavelet estimator
- Latest constraints on primordial non-Gaussianity.
- Conclusions.

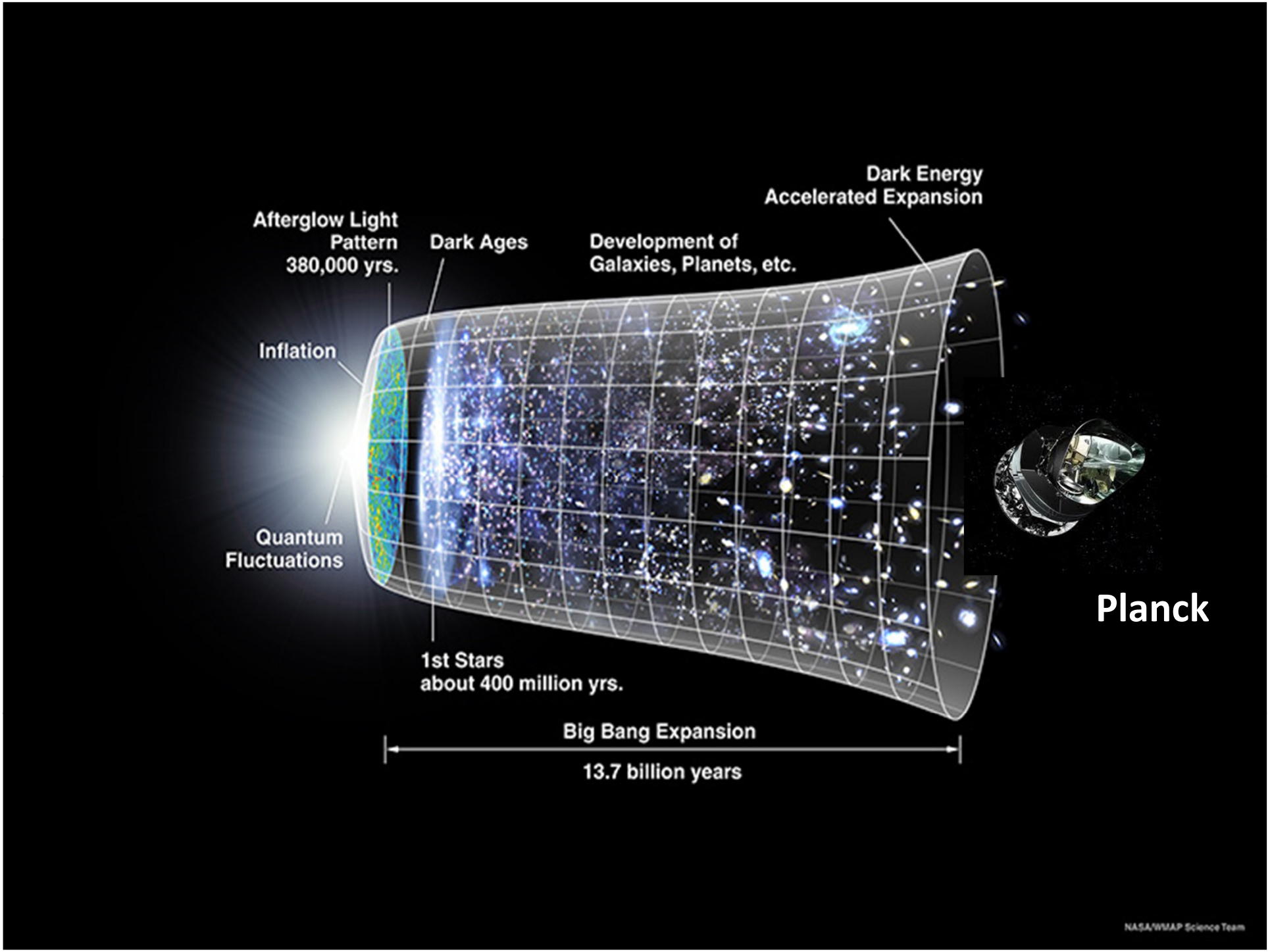
Dark Energy
Accelerated Expansion
Afterglow Light
Pattern
380,000 yrs.
Dark Ages
Development of
Galaxies, Planets, etc.
Inflation
Quantum
Fluctuations
1st Stars
about 400 million yrs.
Big Bang Expansion
13.7 billion years
Planck
NASA/WMAP Science Team

Properties of the CMB anisotropies

- The standard model predicts nearly Gaussian fluctuations for the CMB anisotropies.
- Some sources of non-Gaussian fluctuations:
  - Non-standard inflationary models
  - Topological defects
  - Secondary (non-cosmological) anisotropy sources
  - Contaminants
  - Systematic errors
  - Others

Parametrization of the non-Gaussianity

- A phenomenological way to parametrize the non-Gaussianity is:

$$\Phi = \Phi_L + f_{NL} * \Phi_L^2$$

- Φ_L is the gravitational potential at linear order at the time of recombination (*t = 380,000 yr*).
- f_{NL} is the non-linear coupling parameter. It might have a non-trivial scale dependence, depending on the model.
- This is transferred to the CMB anisotropies through the transfer function.

How can the NG be observed?

- We can identify a Gaussian scalar field by its characteristic odd moments (2n+1) which are equal to zero.
- To measure if there is NG it is easiest to start with the bispectrum.

$$\left\langle \Phi(\vec{k}_1)\Phi(\vec{k}_2)\Phi(\vec{k}_3) \right\rangle = (2\pi)^3 \delta^3(\vec{k}_1 + \vec{k}_2 + \vec{k}_3) F(k_1, k_2, k_3)$$

Shape function

- Different models have different shape functions.
- Reviews on this field:
  - Bartolo et al (2004) arXiv:astro-ph/0406398
  - Yadav & Wandelt (2010) arXiv:1006.0275
  - Liguori et al (2010) arXiv:1001.4707
  - Martinez-Gonzalez & The Planck Collaboration (2012), AIP Conference Proceedings, Volume 1458, pp. 190-206

Local shape

- Shape function:

$$F(k_1,k_2,k_3) = 2\Delta_\Phi^2 f_{nl}\left[\frac{1}{k_1^{3-(n_s-1)}k_2^{3-(n_s-1)}} + \frac{1}{k_1^{3-(n_s-1)}k_3^{3-(n_s-1)}} + \frac{1}{k_2^{3-(n_s-1)}k_3^{3-(n_s-1)}}\right]$$

- This signal peaks in squeezed configurations: $k_1 \approx k_2 >> k_3$
- Inflationary models that generate this shape:
  - multi-field inflationary models
  - the curvaton
  - the inhomogeneous reheating scenario
  - models based on hybrid inflation
  - etc.

$$F(1,x_2,x_3)x_2^2x_3^2 \,/\, F(1,1,1)$$

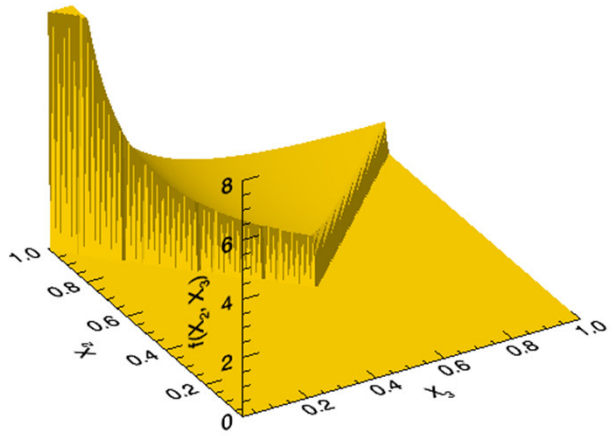

$$x_3 = k_3 / k_1 \qquad x_2 = k_2 / k_1$$

Equilateral shape

- Shape function:

$$F(k_1,k_2,k_3)=6\Delta_\Phi^2 f_{nl}\left[-\frac{1}{k_1^{3-(n_s-1)}k_2^{3-(n_s-1)}}+(2\,perm.)-\frac{2}{(k_1k_2k_3)^{2-2(n_s-1)/3}}+\frac{1}{k_1^{1-(n_s-1)}k_2^{2-(n_s-1)}k_3^{3-(n_s-1)}}+(5\,perm.)\right]$$

- This signal peaks in *equilateral* configurations: $k_1 \approx k_2 \approx k_3$
- Inflationary models that generate this shape:
  - Dirac-Born-Infeld inflation
  - ghost inflation
  - single-field inflationary models in Einstein gravity

$F(1,x_2,x_3)x_2^2x_3^2 / F(1,1,1)$

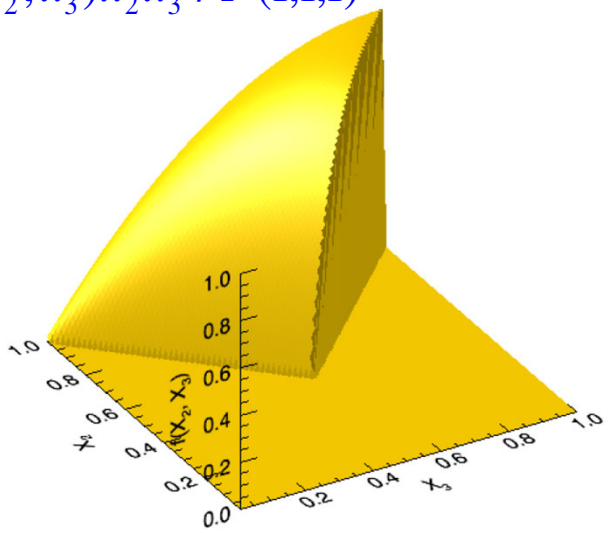

$x_3 = k_3 / k_1$ $\qquad$ $x_2 = k_2 / k_1$

Orthogonal shape

- Shape function:

$$F(k_1,k_2,k_3) = 6Af_{nl} \times \left\{ -\frac{3}{k_1^{4-n_s}k_2^{4-n_s}} - \frac{3}{k_2^{4-n_s}k_3^{4-n_s}} - \frac{3}{k_3^{4-n_s}k_1^{4-n_s}} - \frac{8}{(k_1k_2k_3)^{2(4-n_s)/3}} + \left[\frac{3}{k_1^{4-n_s}k_2^{4-n_s}k_3^{4-n_s}} + (5\ perm.) \right] \right\}$$

- This signal peaks in *equilateral* $k_1 \approx k_2 \approx k_3$ and flat $k_1 = k_2 + k_3$
- Inflationary models that generate this shape:
  - Several single-field inflationary models

$F(1,x_2,x_3)x_2^2x_3^2 / F(1,1,1)$

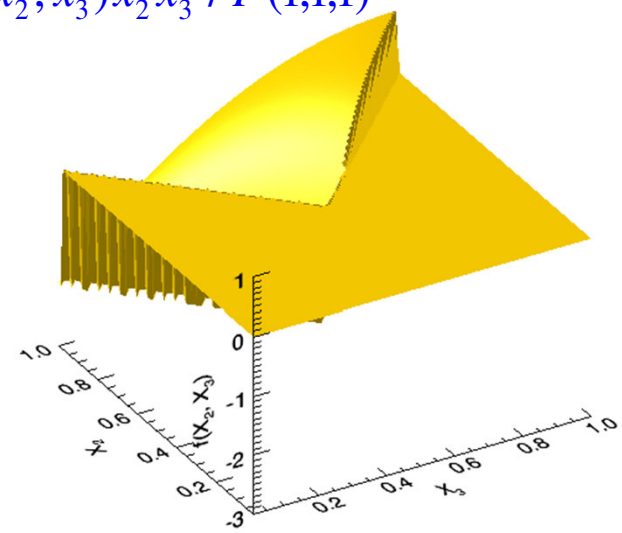

$x_3 = k_3 / k_1$ $\quad$ $x_2 = k_2 / k_1$

Flat shape

- Shape function:

$$F(k_1,k_2,k_3) = 6Af_{nl} \times \left\{ -\frac{3}{k_1^{4-n_s}k_2^{4-n_s}} - \frac{3}{k_2^{4-n_s}k_3^{4-n_s}} - \frac{3}{k_3^{4-n_s}k_1^{4-n_s}} - \frac{8}{(k_1k_2k_3)^{2(4-n_s)/3}} + \left[\frac{3}{k_1^{4-n_s}k_2^{4-n_s}k_3^{4-n_s}} + (5\ perm.) \right] \right\}$$

- This signal peaks in flat $k_1 = k_2 + k_3$ configurations
- Inflationary models that generate this shape:
  - modifications in the initial state of the inflaton field
  - single-field models with high derivative iterations
  - several single-field inflationary models

$$F(1,x_2,x_3)x_2^2x_3^2 \,/\, F(1,1,1)$$

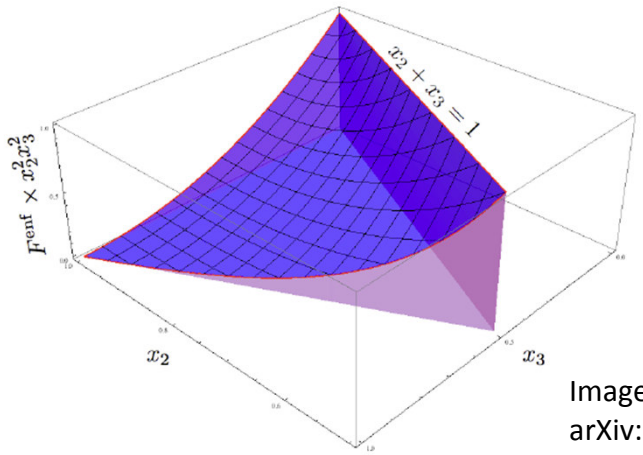

Image from arXiv:0901.4044

Figure 4. The enfolded template shape $F(x_2,x_3) \times x_2^2x_3^2$.

$$x_3 = k_3 / k_1 \qquad x_2 = k_2 / k_1$$

The CMB bispectrum

- The bispectrum of the CMB anisotropies can be given in terms of the shape function $F(k_1, k_2, k_3)$

$$\frac{\Delta T(\hat{n})}{T} = \sum_{\ell m} a_{\ell m} Y_{\ell m}(\hat{n}) \qquad a_{\ell m} = 4\pi(-i)^{\ell} \int \frac{d^3k}{(2\pi)^3} \Phi(\vec{k}) g_{\ell}(k) Y_{\ell m}(\hat{k})$$

$$B_{\ell_1 \ell_2 \ell_3} = \sum_{m_1 m_2 m_3} \begin{pmatrix} \ell_1 & \ell_2 & \ell_3 \\ m_1 & m_2 & m_3 \end{pmatrix} \left\langle a_{\ell_1 m_1} a_{\ell_2 m_2} a_{\ell_3 m_3} \right\rangle$$

$$B_{\ell_1 \ell_2 \ell_3} = b_{\ell_1 \ell_2 \ell_3} \begin{pmatrix} \ell_1 & \ell_2 & \ell_3 \\ 0 & 0 & 0 \end{pmatrix} \sqrt{\frac{(2\ell_1+1)(2\ell_2+1)(2\ell_3+1)}{4\pi}}$$

$$B_{\ell_1 \ell_2 \ell_3} = \sum_{m_1 m_2 m_3} \begin{pmatrix} \ell_1 & \ell_2 & \ell_3 \\ m_1 & m_2 & m_3 \end{pmatrix} \int \frac{d^3k_1}{(2\pi)^3} \frac{d^3k_2}{(2\pi)^3} \frac{d^3k_3}{(2\pi)^3} Y_{\ell_1 m_1}(\hat{k}_1) Y_{\ell_2 m_2}(\hat{k}_2) Y_{\ell_3 m_3}(\hat{k}_3) \times$$

$$\times g_{\ell_1}(k_1) g_{\ell_2}(k_2) g_{\ell_3}(k_3) \left\langle \Phi(k_1) \Phi(k_2) \Phi(k_3) \right\rangle (4\pi)^3 (-i)^{\ell_1+\ell_2+\ell_3}$$

- Local shape:

$$b_{\ell_1\ell_2\ell_3} = 2\int_0^\infty dx x^2 \left[\alpha_{\ell_1}(x)\beta_{\ell 2}(x)\beta_{\ell 3}(x) + (2\,perm)\right]$$

- Equilateral shape:

$$b_{\ell_1\ell_2\ell_3} = 6\int_0^\infty dx x^2 \left[-\alpha_{\ell_1}(x)\beta_{\ell 2}(x)\beta_{\ell 3}(x) + (2\,perm) + \beta_{\ell_1}(x)\gamma_{\ell 2}(x)\delta_{\ell 3}(x) + (5\,perm) - 2\delta_{\ell_1}(x)\delta_{\ell 2}(x)\delta_{\ell 3}(x)\right]$$

- Orthogonal shape:

$$b_{\ell_1\ell_2\ell_3} = 18\int_0^\infty dx x^2 \left[-\alpha_{\ell_1}(x)\beta_{\ell 2}(x)\beta_{\ell 3}(x) + (2\,perm) + \beta_{\ell_1}(x)\gamma_{\ell 2}(x)\delta_{\ell 3}(x) + (5\,perm) - 8/3\,\delta_{\ell_1}(x)\delta_{\ell 2}(x)\delta_{\ell 3}(x)\right]$$

$$\alpha_\ell(x) = \frac{2}{\pi}\int_0^\infty k^2 \mathrm{d}k\, g_{T\ell}(k)\, j_\ell(kx),$$

$$\beta_\ell(x) = \frac{2}{\pi}\int_0^\infty k^2 \mathrm{d}k\, P_\Phi(k) g_{T\ell}(k)\, j_\ell(kx),$$

$$\gamma_\ell(x) = \frac{2}{\pi}\int_0^\infty k^2 \mathrm{d}k\, P_\Phi^{1/3}(k) g_{T\ell}(k)\, j_\ell(kx),$$

$$\delta_\ell(x) = \frac{2}{\pi}\int_0^\infty k^2 \mathrm{d}k\, P_\Phi^{2/3}(k) g_{T\ell}(k)\, j_\ell(kx),$$

See e.g. AC et al (2011) MNRAS, 417, 488-494

Simulating the NG

$$a_{\ell m}^{NG} \equiv \sum_{m_2 m_3 \ell_2 \ell_3} b_{\ell \ell_2 \ell_3} G_{\ell \ell_2 \ell_3}^{m m_2 m_3} \begin{pmatrix} \ell & \ell_2 & \ell_3 \\ m & m_2 & m_3 \end{pmatrix} \frac{\left(a_{\ell_2 m_2}^{G}\right)^*}{C_{\ell_2}} \frac{\left(a_{\ell_3 m_3}^{G}\right)^*}{C_{\ell_3}}$$

Local: $$a_{\ell m}^{NG} = a_{\ell m}^{aBB}$$

Equilateral: $$a_{\ell m}^{NG} = -3a_{\ell m}^{aBB} - 2a_{\ell m}^{dDD} + 6a_{\ell m}^{gBD}$$

Orthogonal: $$a_{\ell m}^{NG} = -9a_{\ell m}^{aBB} - 8a_{\ell m}^{dDD} + 18a_{\ell m}^{gBD}$$

$$a_{\ell m}^{aBB} = \int_0^\infty dx x^2 \alpha_\ell(x) \int d^2\hat{n} Y_{\ell m}^*(\hat{n}) M_\beta(x,\hat{n}) M_\beta(x,\hat{n})$$

$$a_{\ell m}^{dDD} = \int_0^\infty dx x^2 \delta_\ell(x) \int d^2\hat{n} Y_{\ell m}^*(\hat{n}) M_\delta(x,\hat{n}) M_\delta(x,\hat{n})$$

$$a_{\ell m}^{gBD} = \int_0^\infty dx x^2 \gamma_\ell(x) \int d^2\hat{n} Y_{\ell m}^*(\hat{n}) M_\beta(x,\hat{n}) M_\delta(x,\hat{n})$$

$$M_\alpha(x,\hat{n}) = \sum_{\ell m} a_{\ell m}^G \alpha_\ell(x) \frac{Y_{\ell m}(\hat{n})}{C_\ell}$$

$$M_\beta(x,\hat{n}) = \sum_{\ell m} a_{\ell m}^G \beta_\ell(x) \frac{Y_{\ell m}(\hat{n})}{C_\ell}$$

$$M_\gamma(x,\hat{n}) = \sum_{\ell m} a_{\ell m}^G \gamma_\ell(x) \frac{Y_{\ell m}(\hat{n})}{C_\ell}$$

$$M_\delta(x,\hat{n}) = \sum_{\ell m} a_{\ell m}^G \delta_\ell(x) \frac{Y_{\ell m}(\hat{n})}{C_\ell}$$

Non-Gaussian simulations

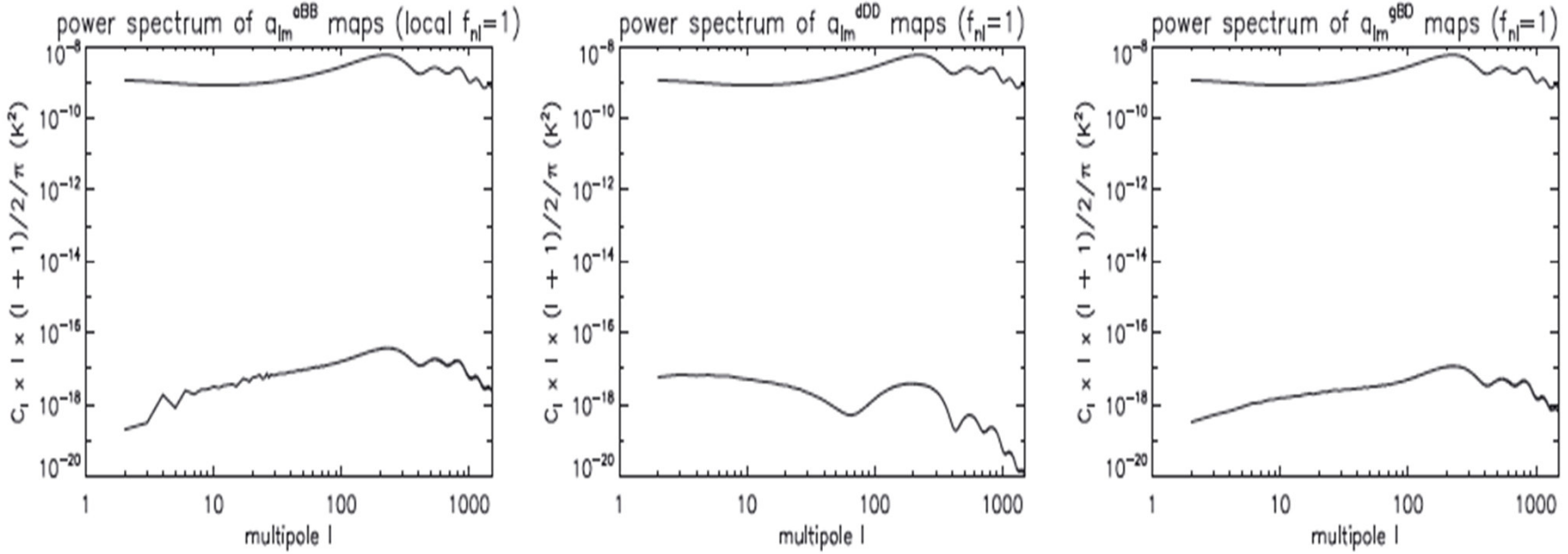

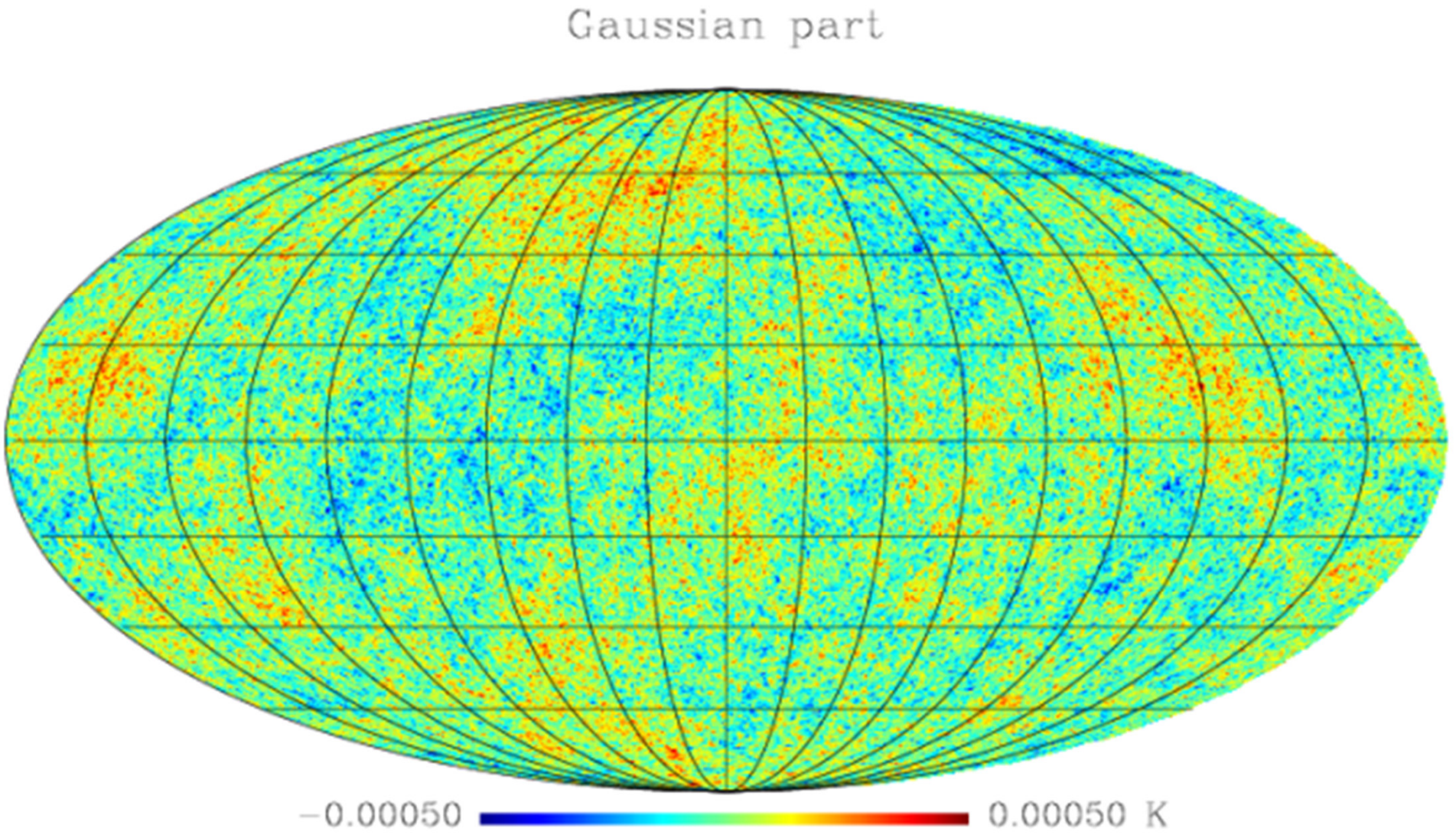
Gaussian part
−0.00050
0.00050 K

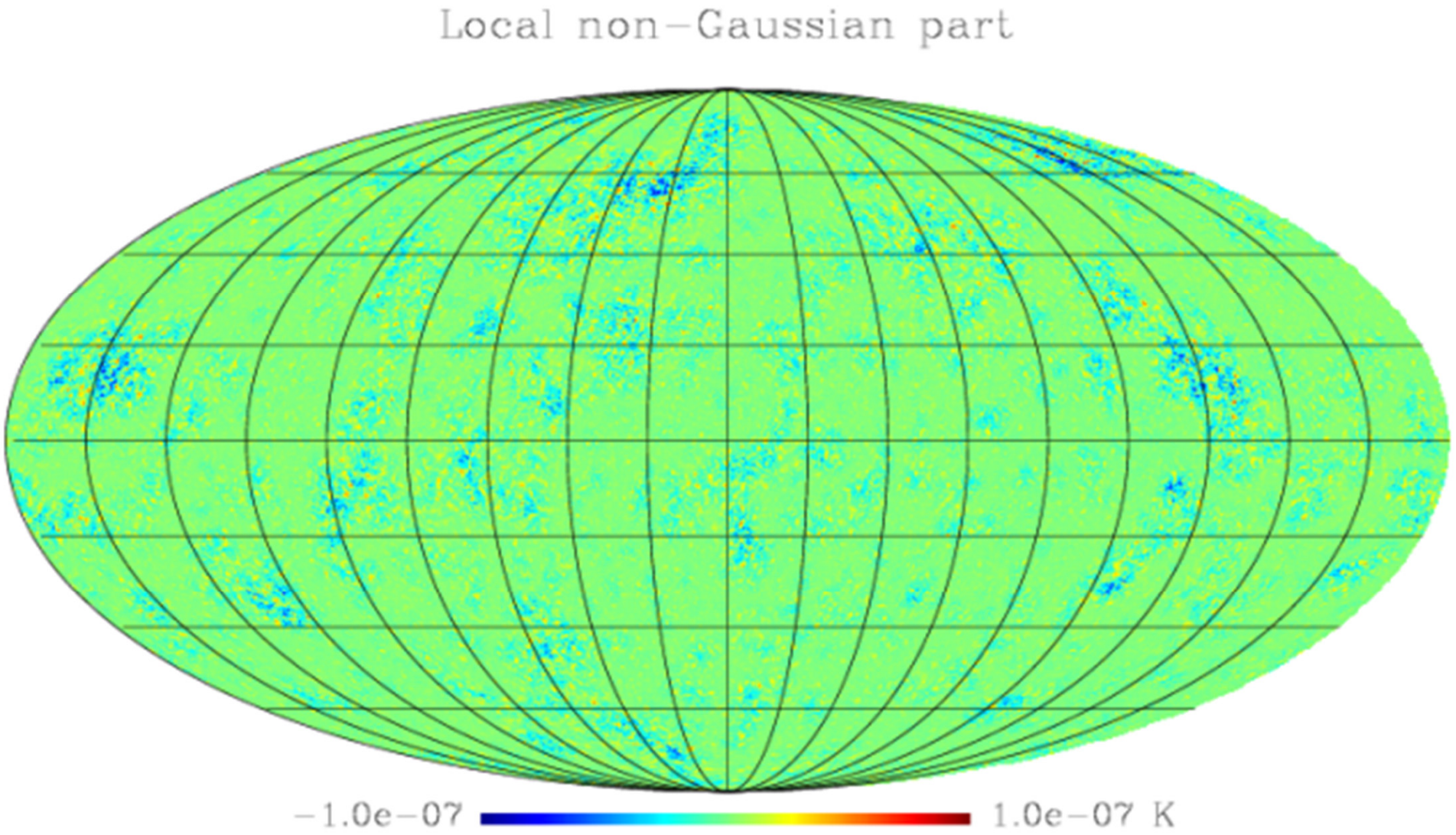
Local non−Gaussian part
−1.0e−07
1.0e−07 K

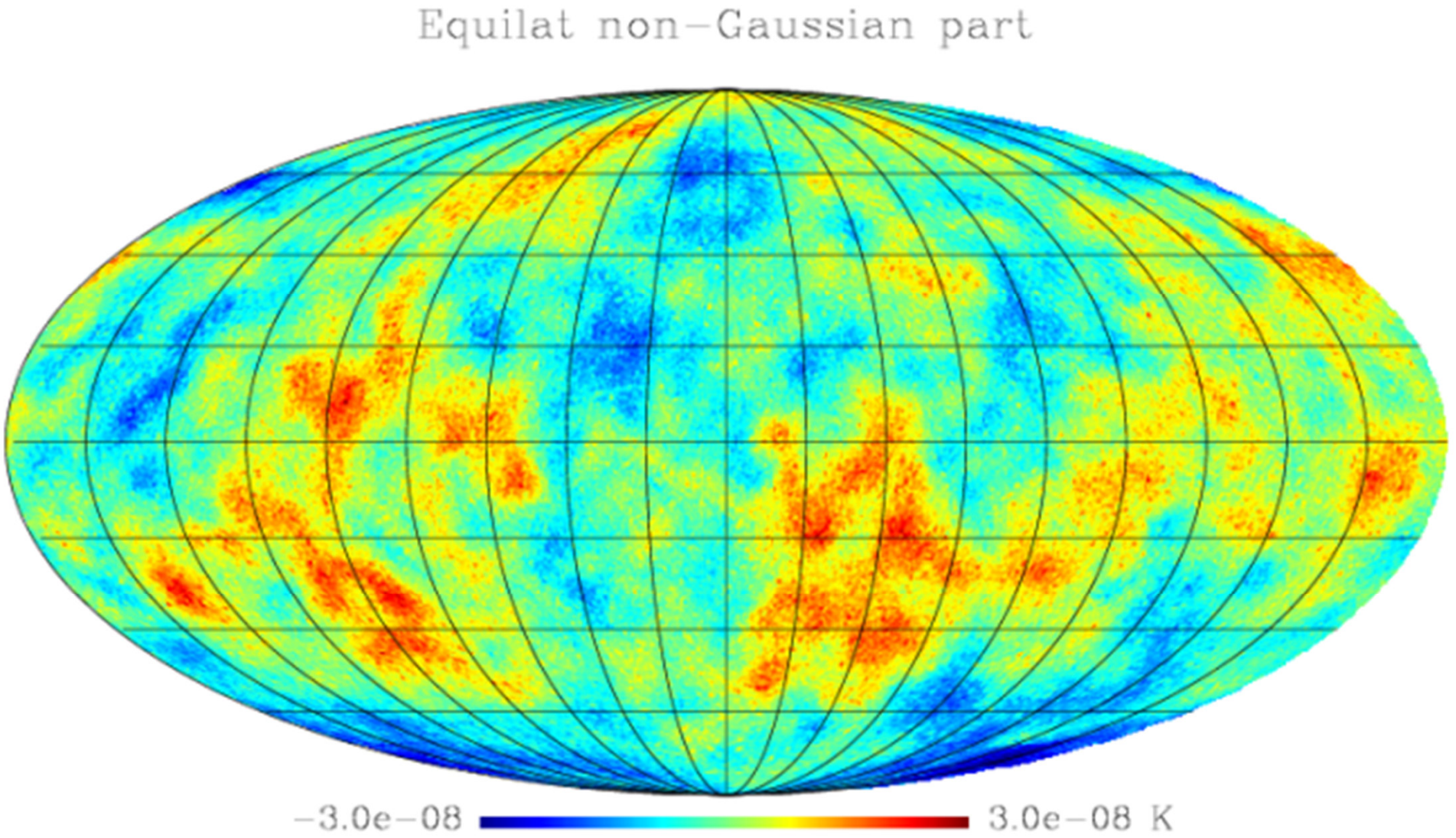
Equilat non−Gaussian part
−3.0e−08
3.0e−08 K

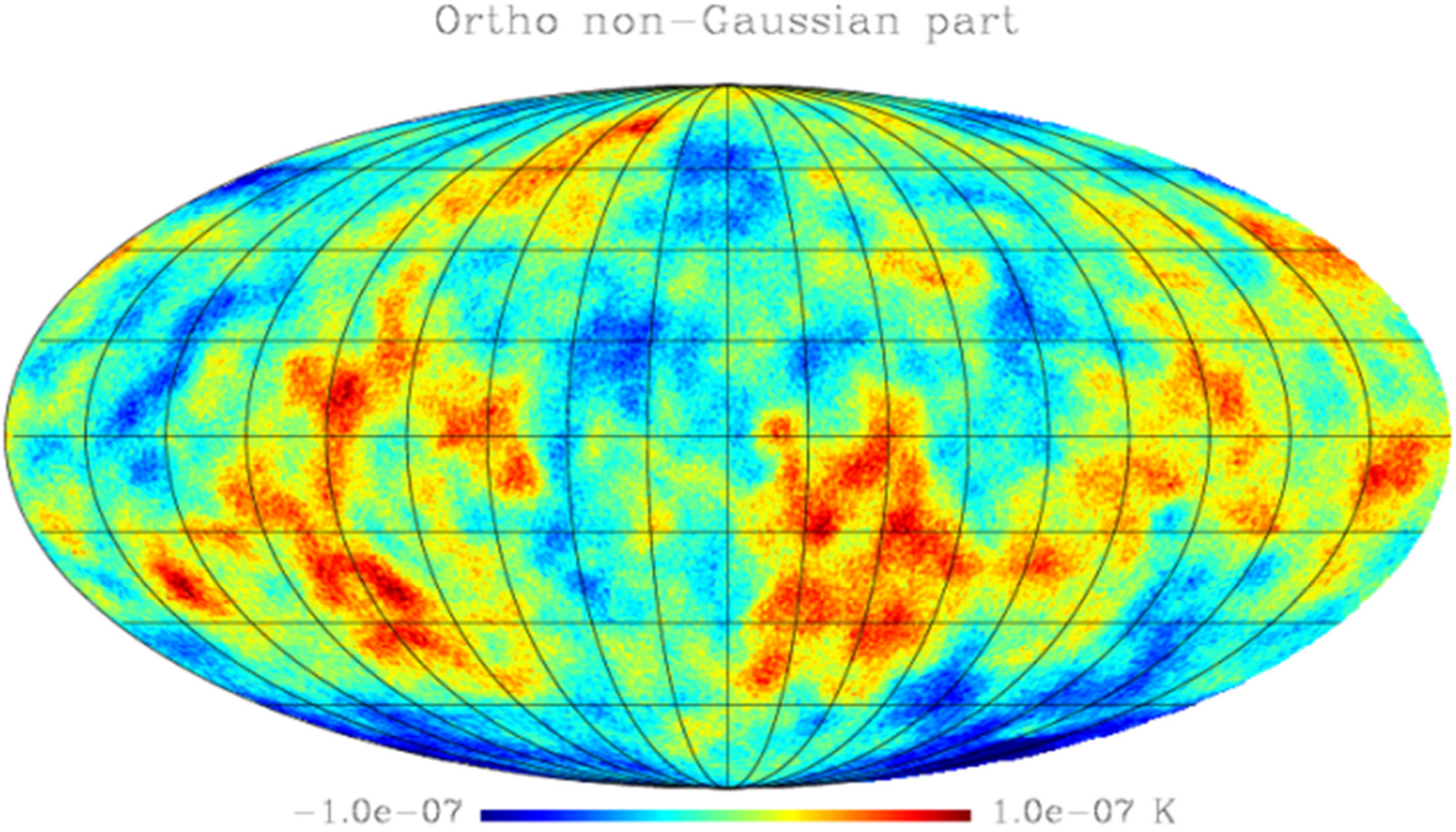
Ortho non−Gaussian part
−1.0e−07
1.0e−07 K

Contaminants that bias the f_{nl} estimation

The unresolved point sources produce a particular bispectrum

- Low frequencies (< 100 GHz): radio sources are dominated by blazars (AGN-powered sources with flat spectrum at GHz)
- High frequencies (> 200 GHz): infra-red sources dominated by spiral or starburst galaxies, high z sources, etc.

See AC, Tucci, et al (2013)

The interplay between gravitational lensing and the ISW effect produces a particular bispectrum:

$$b_{\ell_1\ell_2\ell_3}^{ISW-lensing} = \left\{ \frac{\ell_2(\ell_2+1)-\ell_1(\ell_1+1)-\ell_3(\ell_3+1)}{2} C_{\ell_1}^{T\psi} C_{\ell_3}^{TT} + 5perm \right\}$$

See Hanson, Smith, Challinor & Liguori (2009) and Lewis, Challinor & Hanson (2011) for more details

The PS bispectrum

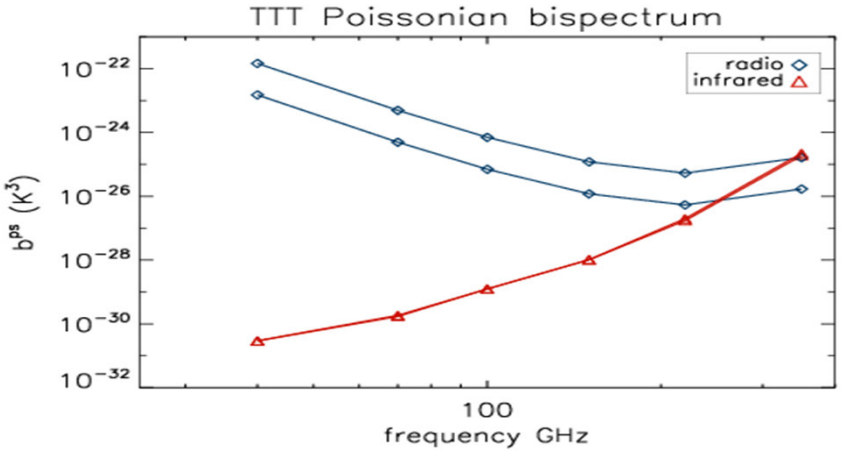

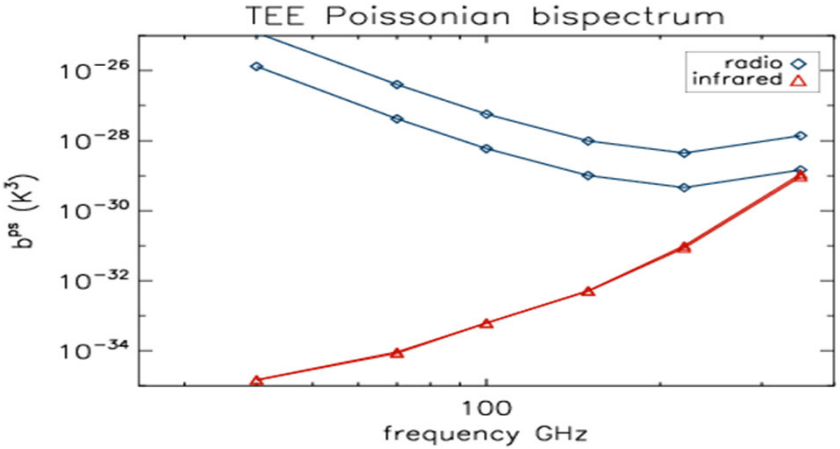

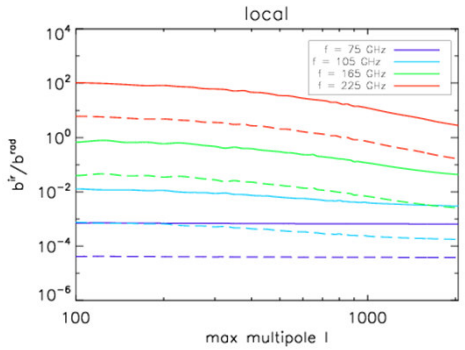

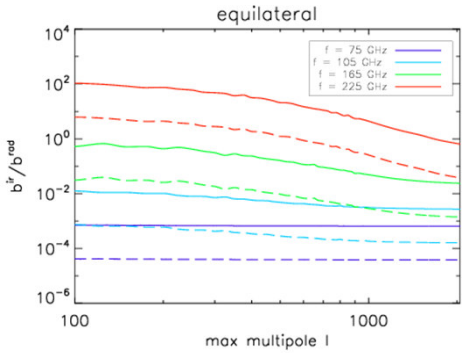

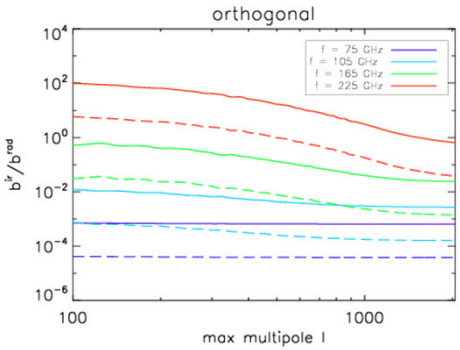

$$B^{PS}_{\ell_1\ell_2\ell_3} = B^{radio} + B^{ir,poiss}\sqrt{\frac{C^{ir}_{\ell_1}C^{ir}_{\ell_2}C^{ir}_{\ell_3}}{C^{ir,poiss}_{\ell_1}C^{ir,poiss}_{\ell_2}C^{ir,poiss}_{\ell_3}}}$$

The bispectrum including polarization can be defined in an equivalent way (considered components **TTT, TEE, TBB**). The remaining components are equal to zero.

Primordial non-Gaussianity f_{nl} bias estimator (T)

$$\Delta f_{nl} = \frac{\sum_{\ell_1 \le \ell_2 \le \ell_3 \le \ell_{\max}} \frac{B^{ps}_{\ell_1\ell_2\ell_3} B^{prim}_{\ell_1\ell_2\ell_3}}{\Delta_{\ell_1\ell_2\ell_3} C_{\ell_1} C_{\ell_2} C_{\ell_3}}}{\sum_{\ell_1 \le \ell_2 \le \ell_3 \le \ell_{\max}} \frac{B^{prim}_{\ell_1\ell_2\ell_3} B^{prim}_{\ell_1\ell_2\ell_3}}{\Delta_{\ell_1\ell_2\ell_3} C_{\ell_1} C_{\ell_2} C_{\ell_3}}} \qquad \sigma^2(f_{nl}) = \frac{1}{\sum_{\ell_1 \le \ell_2 \le \ell_3 \le \ell_{\max}} \frac{B^{prim}_{\ell_1\ell_2\ell_3} B^{prim}_{\ell_1\ell_2\ell_3}}{\Delta_{\ell_1\ell_2\ell_3} C_{\ell_1} C_{\ell_2} C_{\ell_3}}}$$

Total power spectrum

$$C_\ell = \left(C_\ell^{CMB} + C_\ell^{IR\,PS} + C_\ell^{Radio\,PS}\right) b_\ell^2 w_\ell^2 + C_\ell^{noise}$$

CMB power spectrum

Infra-red point source power spectrum

radio point source power spectrum

Instrumental noise

Primordial non-Gaussianity f_{nl} bias estimator (T and E)

$$\Delta f_{nl} = \frac{\sum_{ijk,rst,\ell_1\le\ell_2\le\ell_3\le\ell_{\max}} B^{ijk,ps}_{\ell_1\ell_2\ell_3} C^{-1}_{ijk,rst} B^{rst,prim}_{\ell_1\ell_2\ell_3}}{\sum_{ijk,rst,\ell_1\le\ell_2\le\ell_3\le\ell_{\max}} B^{ijk,prim}_{\ell_1\ell_2\ell_3} C^{-1}_{ijk,rst} B^{rst,prim}_{\ell_1\ell_2\ell_3}} \qquad \sigma^2(f_{nl}) = \frac{1}{\sum_{ijk,rst,\ell_1\le\ell_2\le\ell_3\le\ell_{\max}} B^{prim}_{\ell_1\ell_2\ell_3} C^{-1}_{ijk,rst} B^{prim}_{\ell_1\ell_2\ell_3}}$$

Indices i, j, k, r, s, t = {T, E}

Power spectrum covariance

$$C_{ijk,pqr} = C^{ip}_{\ell_1} C^{jq}_{\ell_2} C^{kr}_{\ell_3} + C^{ip}_{\ell_1} C^{jr}_{\ell_2} C^{kq}_{\ell_3} \delta_{\ell_2\ell_3} + C^{ir}_{\ell_1} C^{jq}_{\ell_2} C^{kp}_{\ell_3} \delta_{\ell_1\ell_3} + C^{iq}_{\ell_1} C^{jp}_{\ell_2} C^{kr}_{\ell_3} \delta_{\ell_1\ell_2} +$$
$$+ C^{iq}_{\ell_1} C^{jr}_{\ell_2} C^{kp}_{\ell_3} \delta_{\ell_1\ell_2} \delta_{\ell_2\ell_3} \delta_{\ell_1\ell_3} + C^{ir}_{\ell_1} C^{jp}_{\ell_2} C^{kq}_{\ell_3} \delta_{\ell_1\ell_3} \delta_{\ell_2\ell_1} \delta_{\ell_2\ell_3}$$

Polarization non-zero point source power spectrum and bispectrum (even number of E)

$$b^{TEE} = \langle p^2 \rangle \langle \cos^2(2\phi) \rangle b^{TTT} \qquad b^{TTE} = b^{EEE} = 0$$

Expected uncertainties in f_{nl}

AC, M. Tucci et al. (2013) (arXiv:1301.1544)

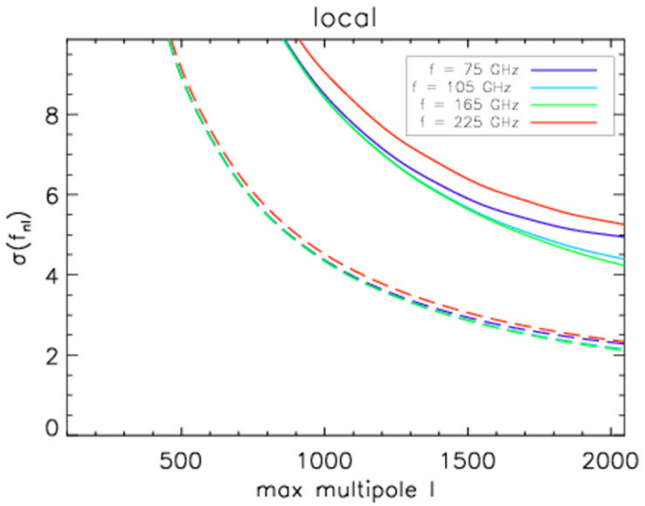

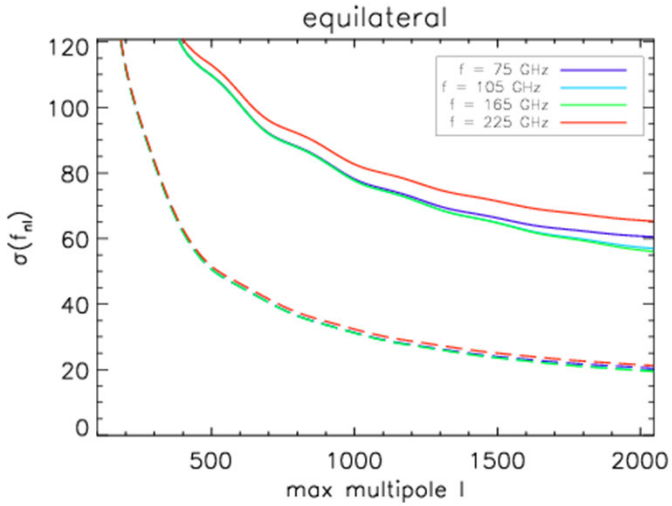

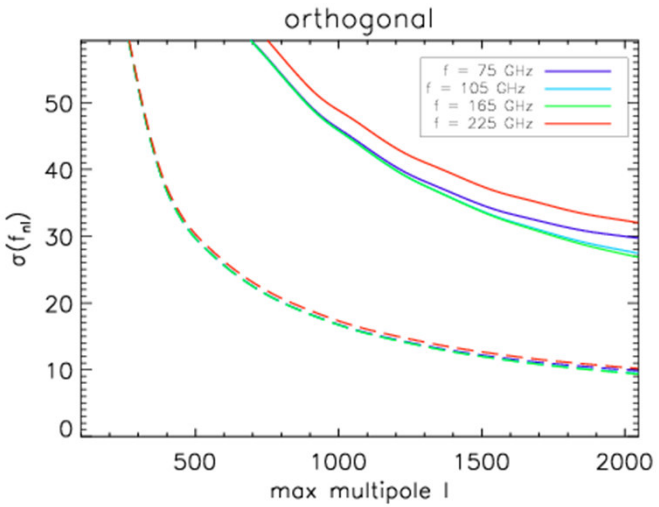

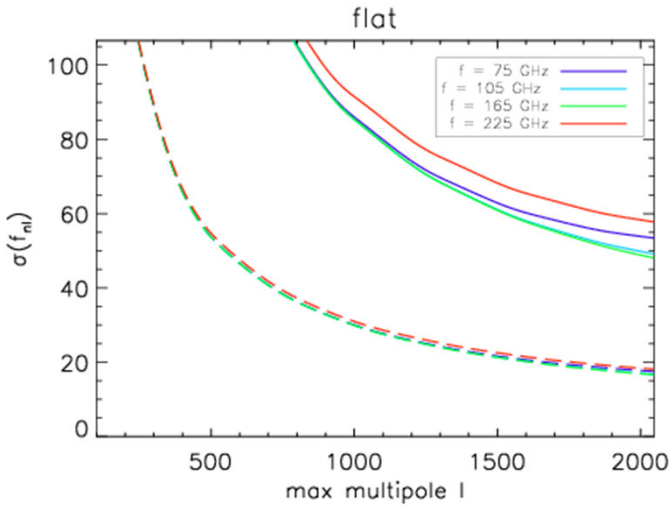

Point source contamination to f_{nl}

AC, M. Tucci et al. (2013)

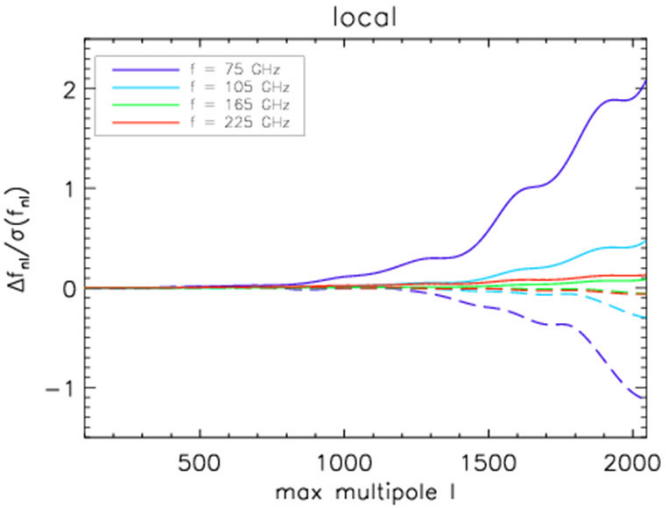

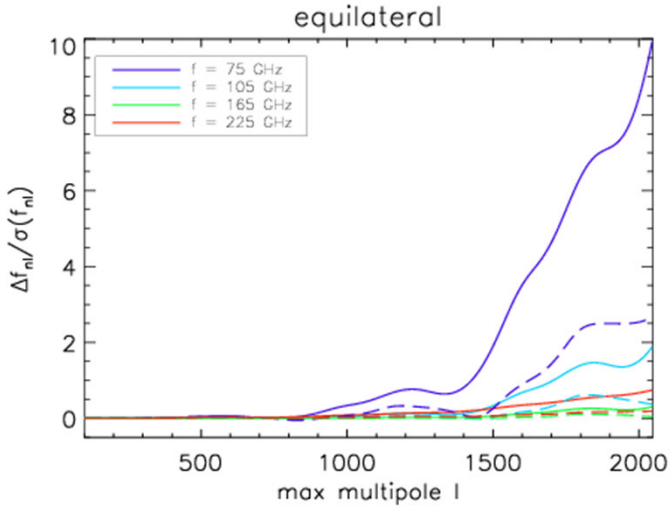

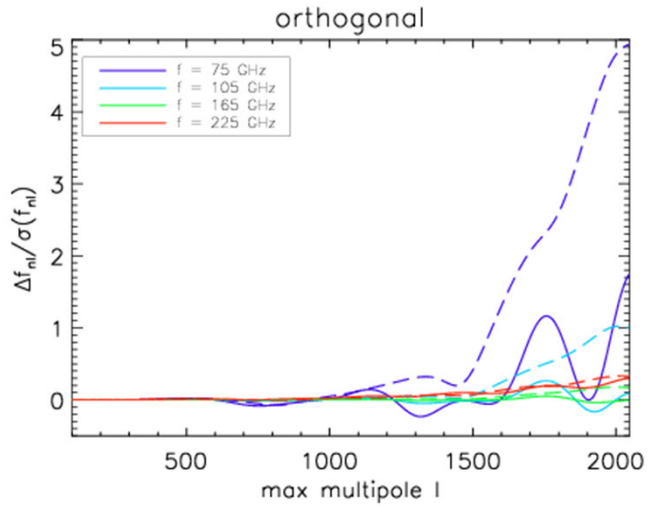

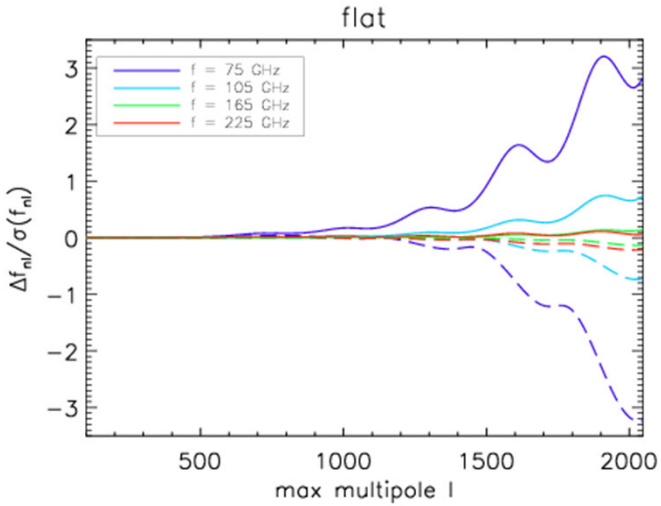

Table 2. The expected uncertainty $\sigma(f_{nl})$, bias Δf_{nl} and relative bias $\Delta f_{nl}/\sigma(f_{nl})$ at $\ell_{max} = 2048$ from temperature only and temperature plus polarization for an ideal mission. S_c =0.3Jy is taken.

	case	T	T	T	T	T	T	T+E	T+E	T+E	T+E	T+E	T+E
	Freq.	45	75	105	165	225	375	45	75	105	165	225	375
local	$\sigma(f_{nl})$	7.4	4.9	4.4	4.2	5.2	29.7	2.8	2.3	2.1	2.1	2.3	3.3
	Δf_{nl}	82.1	10.3	2.1	0.4	0.7	25.6	-9.7	-2.6	-0.6	-0.1	-0.1	-0.1
	$\Delta f_{nl}/\sigma(f_{nl})$	11.1	2.1	0.5	0.1	0.1	0.9	-3.5	-1.1	-0.3	-0.1	-0.1	-0.0
equilateral	$\sigma(f_{nl})$	75.4	60.4	56.8	55.9	65.1	232.4	24.0	20.3	19.5	19.2	21.1	35.3
	Δf_{nl}	4629.3	599.9	107.2	17.2	49.1	950.7	480.2	54.5	7.3	0.8	4.0	17.9
	$\Delta f_{nl}/\sigma(f_{nl})$	61.4	9.9	1.9	0.3	0.8	4.1	20.0	2.7	0.4	0.0	0.2	0.5
orthogonal	$\sigma(f_{nl})$	40.1	29.7	27.4	26.8	32.0	139.0	11.6	9.8	9.4	9.2	10.1	16.5
	Δf_{nl}	955.5	51.7	2.5	-0.2	9.7	371.4	308.7	48.3	9.4	1.6	3.4	7.2
	$\Delta f_{nl}/\sigma(f_{nl})$	23.8	1.7	0.1	-0.0	0.3	2.7	26.7	4.9	1.0	0.2	0.3	0.4
flat	$\sigma(f_{nl})$	73.7	53.3	49.0	47.9	57.6	284.7	20.6	17.4	16.6	16.4	17.9	29.1
	Δf_{nl}	598.6	150.5	36.0	6.7	3.4	-66.0	-311.6	-56.3	-12.2	-2.2	-3.9	-5.2
	$\Delta f_{nl}/\sigma(f_{nl})$	8.1	2.8	0.7	0.1	0.1	-0.2	-15.1	-3.2	-0.7	-0.1	-0.2	-0.2

AC, M. Tucci et al. (2013) (arXiv:1301.1544)

Expected PS bias for Planck

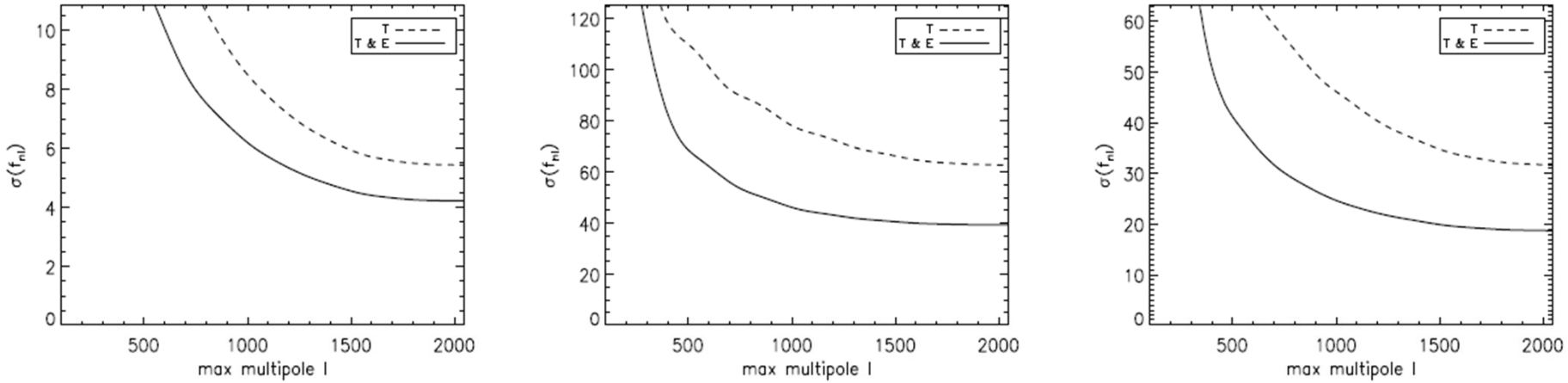

FIGURE 4. The f_{nl} error-bars obtained from the Fisher matrix for the local *(left)*, equilateral *(middle)*, and orthogonal *(right)* cases. The maximum expected precision for the cosmological *Planck* channels using only intensity information is $\sigma(f_{nl}^{loc}) \sim 5$, $\sigma(f_{nl}^{eq}) \sim 65$ and $\sigma(f_{nl}^{ort}) \sim 30$. Adding polarization the maximum expected precision is $\sigma(f_{nl}^{loc}) \sim 4.2$, $\sigma(f_{nl}^{eq}) \sim 39.4$ and $\sigma(f_{nl}^{ort}) \sim 18.7$. Unofficial Planck results, credits: the presenters of this contribution.

Shape	Local	Equilateral	Orthogonal
Point source $\Delta(f_{nl})$ (T Only)	0.3	15	1.7
Point source $\Delta(f_{nl})$ (T & E)	0.03	5.4	2.0

[4] We consider a Gaussian beam with $FWHM = 7.2$ arcmin, an instrumental noise $\sigma_{noise} = 20.1$ μK·arcmin for T and $\sigma_{noise} = 33.3$ μK·arcmin for E corresponding to the *Planck* 143 GHz band.

Martínez-González & The Planck Collaboration (2012)

Lensing contamination

$$\hat{A} \equiv \frac{\sum_{\ell_1 \le \ell_2 \le \ell_3 \le \ell_{\max}} \frac{B^{ISWL}_{\ell_1\ell_2\ell_3} \hat{B}^{obs}_{\ell_1\ell_2\ell_3}}{\Delta_{\ell_1\ell_2\ell_3} C_{\ell_1} C_{\ell_2} C_{\ell_3}}}{\sum_{\ell_1 \le \ell_2 \le \ell_3 \le \ell_{\max}} \frac{B^{ISWL}_{\ell_1\ell_2\ell_3} B^{ISWL}_{\ell_1\ell_2\ell_3}}{\Delta_{\ell_1\ell_2\ell_3} C_{\ell_1} C_{\ell_2} C_{\ell_3}}}$$

$$\Delta f_{nl} = \frac{\sum_{\ell_1 \le \ell_2 \le \ell_3 \le \ell_{\max}} \frac{B^{ISWL}_{\ell_1\ell_2\ell_3} B^{prim}_{\ell_1\ell_2\ell_3}}{\Delta_{\ell_1\ell_2\ell_3} C_{\ell_1} C_{\ell_2} C_{\ell_3}}}{\sum_{\ell_1 \le \ell_2 \le \ell_3 \le \ell_{\max}} \frac{B^{prim}_{\ell_1\ell_2\ell_3} B^{prim}_{\ell_1\ell_2\ell_3}}{\Delta_{\ell_1\ell_2\ell_3} C_{\ell_1} C_{\ell_2} C_{\ell_3}}}$$

Ideally this amplitude should be A = 1

Lewis, Challinor & Hanson (2011) forecasts for local shape with Planck

	$\sigma_{f_{\rm NL}}$	$\sigma_{\rm lens}$	correlation	bias on $f_{\rm NL}$	$\sigma^{\rm marge}_{f_{\rm NL}}$
T	4.31	0.19	0.24	9.5	4.44
T+E	2.14	0.12	0.022	2.6	2.14
Planck T	5.92	0.26	0.22	6.4	6.06
Planck T+E	5.19	0.22	0.13	4.3	5.23

Table 1. Errors and biases on CMB lensing and primordial local-model non-Gaussianity parameterized by $f_{\rm NL}$ for Planck-like noise (assuming isotropic coverage over the full sky with sensitivity $\Delta T = \Delta Q/2 = \Delta U/2 = 50\,\mu$K arcmin [$N_l^T = N_l^{Q/U}/4 = 2 \times 10^{-4}\mu{\rm K}^2$] and a beam FWHM of 7 arcmin) or cosmic-variance limited data with $l_{\rm max} = 2000$. From eq. (5.35) the errors $\sigma_{f_{\rm NL}}$ and $\sigma_{\rm lens}$ are the errors on the amplitudes of the corresponding bispectrum templates individually when the other one is fixed; $\sigma^{\rm marge}_{f_{\rm NL}}$ is the Fisher error on $f_{\rm NL}$ if the amplitude of the lensing contribution is marginalized over; and the correlation is that between the two bispectrum shapes. The bias is the systematic error on $f_{\rm NL}$ if the CMB lensing contribution is neglected, i.e. eq. (5.26).

Estimating the non-Gaussianity

- Minkowski functionals
- Wavelets
- Bispectrum-based estimators: KSW, binned, modal, etc
- Etc.

Minkowski functionals

- Area: A(ν)
  - The area of the hot spots above a given threshold (ν)
- Contour Length : C(ν)
  - The perimeter of the hot spots above a given threshold (ν)
- Genus : G(ν)
  - Number of hot spots (> ν) minus number of cold spots (< ν)

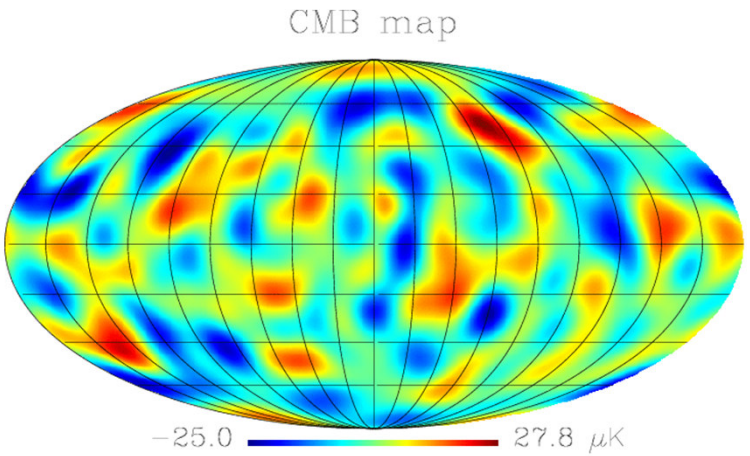

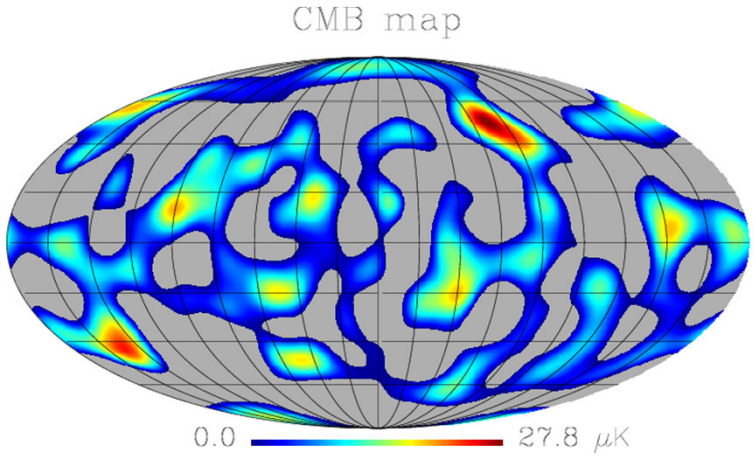

Bispectrum-based estimators

- KSW (Komatsu-Spergel-Wandelt)

$$\hat{f}_{nl}^{cub} = \int_0^\infty dx x^2 \int d^2\hat{n} Y_{\ell m}^*(\hat{n}) M_\alpha(x,\hat{n}) M_\beta^2(x,\hat{n})$$

- Binned

$$T_i(\hat{n}) = \sum_{\ell\in\Delta_i}\sum_m a_{\ell m} Y_{\ell m}(\hat{n}) \qquad B_{i_1 i_2 i_3} = \int d^2\hat{n} T_{i_1}(\hat{n}) T_{i_2}(\hat{n}) T_{i_3}(\hat{n})$$

- Modal

$$\hat{f}_{nl}^{cub} = \frac{1}{N^2}\sum_{prs}\alpha_{prs}\int d^2\hat{n} M_p(\hat{n}) M_r(\hat{n}) M_s(\hat{n}) \qquad M_p(\hat{n}) = \sum_{\ell m} q_p(\ell) a_{\ell m} \frac{Y_{\ell m}(\hat{n})}{\sqrt{C_\ell}}$$

All the estimators need a linear correction to minimise the uncertainties due to incomplete sky cut, noise anisotropies, etc.

The spherical Mexican hat wavelet

- The spherical Mexican hat wavelet (SMHW):

position → , ← scale

$$\Psi_S(\vec{x};\vec{b},R)$$

translation →

$$\Psi_S(\theta;R)=\frac{1}{\sqrt{2\pi}N(R)}\left[1+\left(\frac{y}{2}\right)^2\right]^2\left[2-\left(\frac{y}{R}\right)^2\right]e^{-y^2/(2R^2)}$$

$$y=2\tan(\theta/2)$$

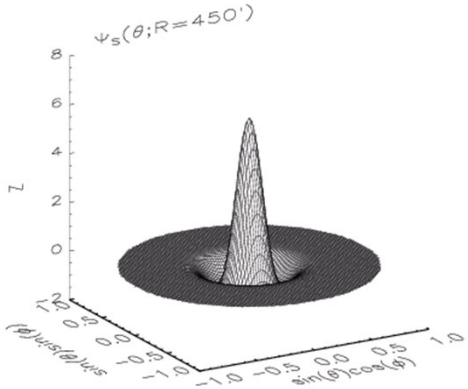

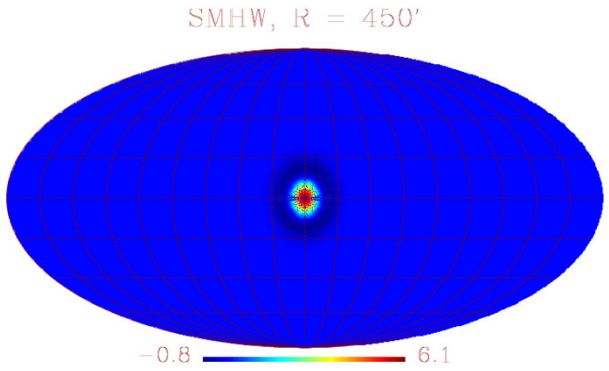

- Continuous wavelet transform:

$$w(\vec{b};R)=\int d\vec{n} f(\vec{n})\Psi(\vec{n};\vec{b},R)$$

$$w(\vec{b};R)=\sum_{lm} b_l(R)a_{lm}Y_{lm}(\theta,\varphi)$$

f_{nl} estimates using wavelets

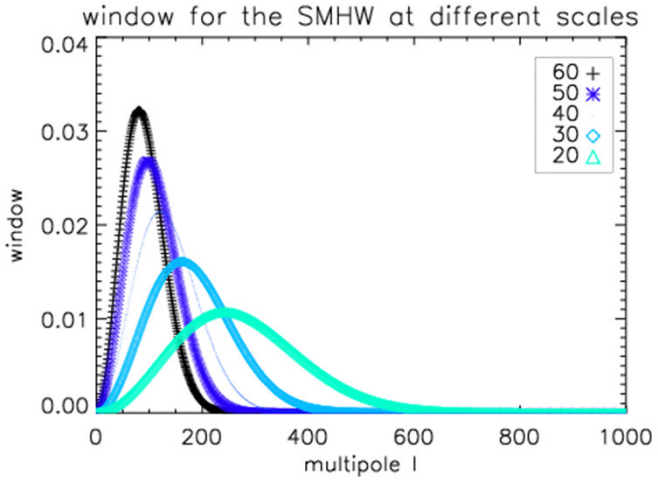

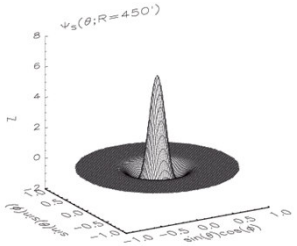

Wavelet: spherical Mexican hat wavelet (SMHW)

References:

Martínez-González et al. (2002) arXiv:astro-ph/0111284

Mukherjee & Wang (2004) arXiv:astro-ph/0402602

Curto et al. (2009) arXiv:0902.1523

Curto et al. (2012) arXiv:1111.3390

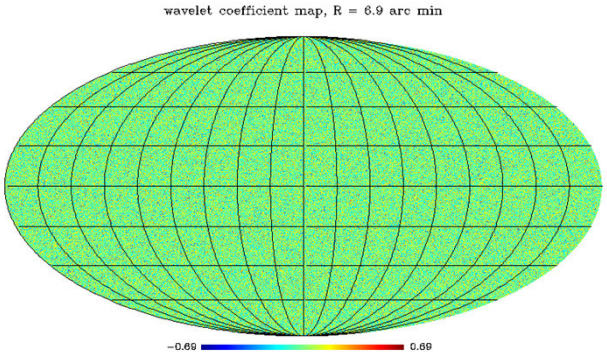

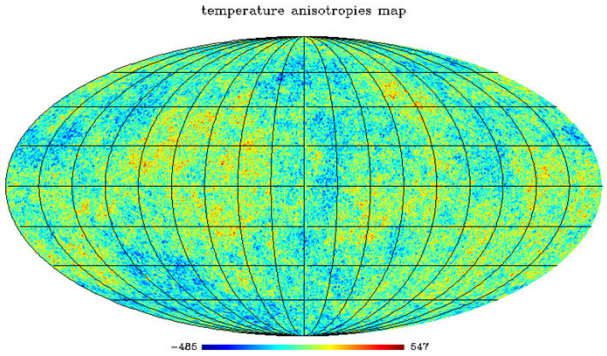

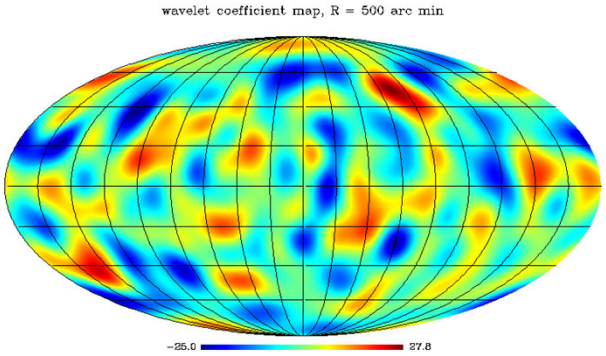

List of 16 selected angular scales in arcmin

0	**1.3**	**2.1**	**3.4**	**5.4**	**8.7**	**13.9**	**22.3**
35.6	**57**	**91.2**	**146**	**233.5**	**373.6**	**597.7**	**956.3**

Cubic statistics with the wavelet

- Select a characteristic set of angular scales R_j.
- Compute the wavelet transform map $w(b_i,R_j)$ at these scales R_j.
- Compute third order statistics by combining different scales:

$$q_{ijk} = \frac{1}{\sigma_i \sigma_j \sigma_k} \int w(\vec{b}, R_i) w(\vec{b}, R_j) w(\vec{b}, R_k) d\vec{b}$$

Arxiv:1007.2181

- Combine in a χ^2 test all the estimators:

$$\chi^2(f_{nl}) = \sum_{ijk,rst} (q_{ijk} - \langle q_{ijk} \rangle_{f_{nl}}) C^{-1}_{ijk,rst} (q_{rst} - \langle q_{rst} \rangle_{f_{nl}})$$

data

f_{nl} model

Results on f_{nl} estimation with WMAP data

Shape	Local	Equilateral	Orthogonal
Data best fitting f_{nl}	39	-63	-160
$\sigma(f_{nl})$	22	145	106
Point source $\Delta(f_{nl})$	2	37	25

Results with the SMHW, AC et al (2011), arXiv:1105.6106 & AC et al (2012), (arXiv:1111.3390).

Shape	Local	Equilateral	Orthogonal
Data best fitting f_{nl}	32	26	-202
$\sigma(f_{nl})$	21	140	104
Point source $\Delta(f_{nl})$	2	22	-

Results from WMAP collaboration, Komatsu et al. (2011), arXiv:1001.4538.

Planck f_{nl} estimates using wavelets

Wavelet: spherical Mexican hat wavelet:

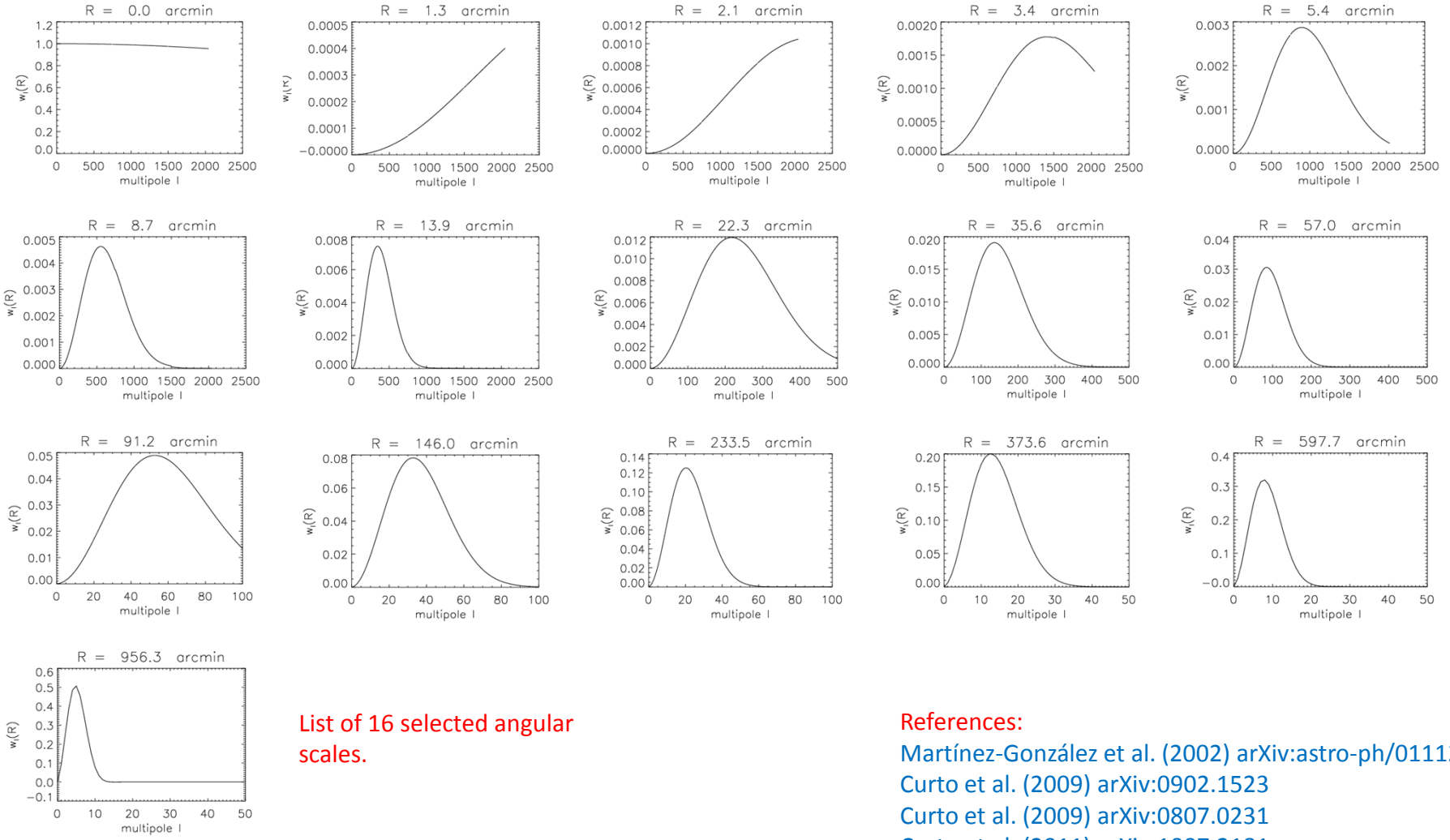

List of 16 selected angular scales.

References:

Martínez-González et al. (2002) arXiv:astro-ph/0111284
Curto et al. (2009) arXiv:0902.1523
Curto et al. (2009) arXiv:0807.0231
Curto et al. (2011) arXiv:1007.2181
Curto et al. (2011) arXiv:1105.6106
Curto et al. (2012) arXiv:1111.3390

Planck cleaned data

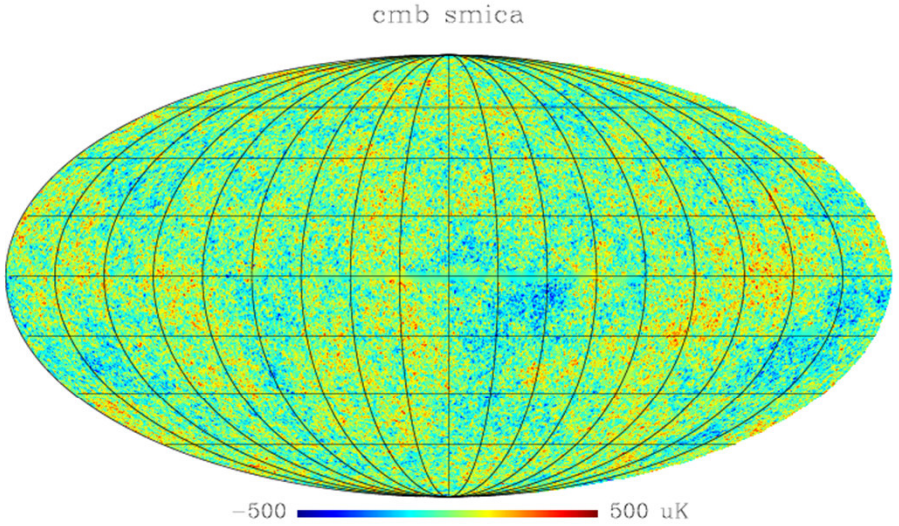

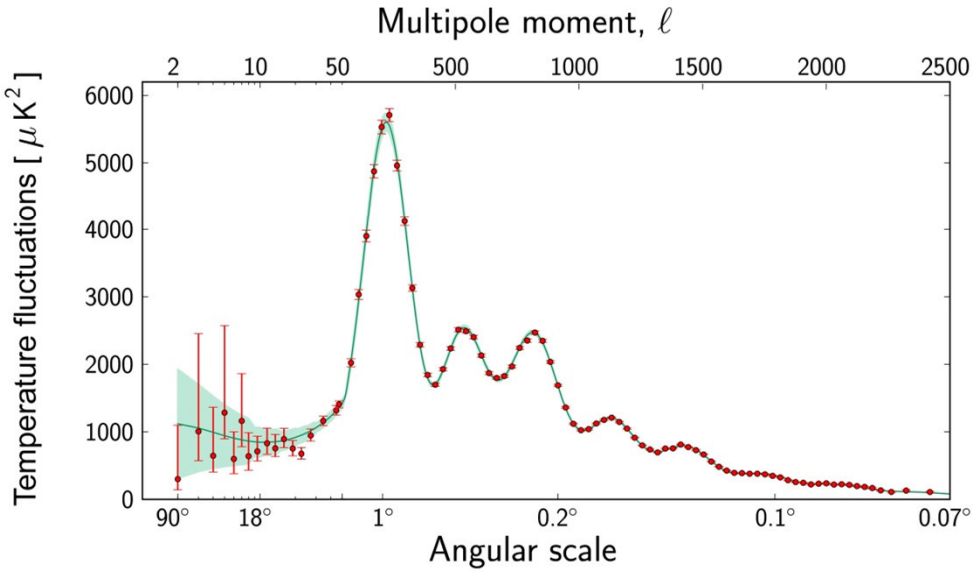

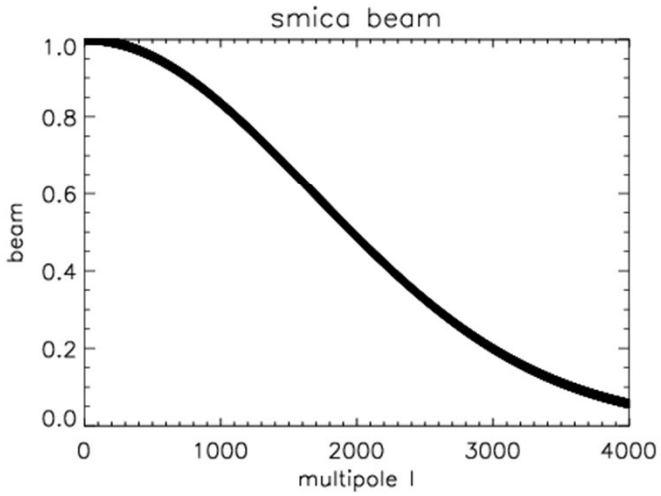

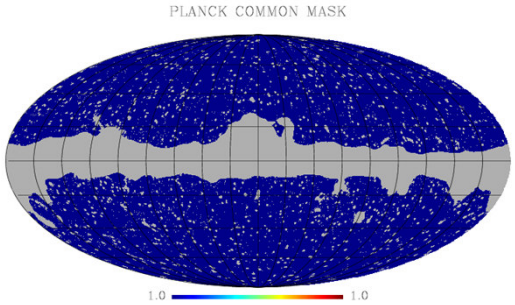

The Mask

- No pre-processing of data through inpainting of the point source mask.
- As a consequence the estimator becomes hardly less optimal.

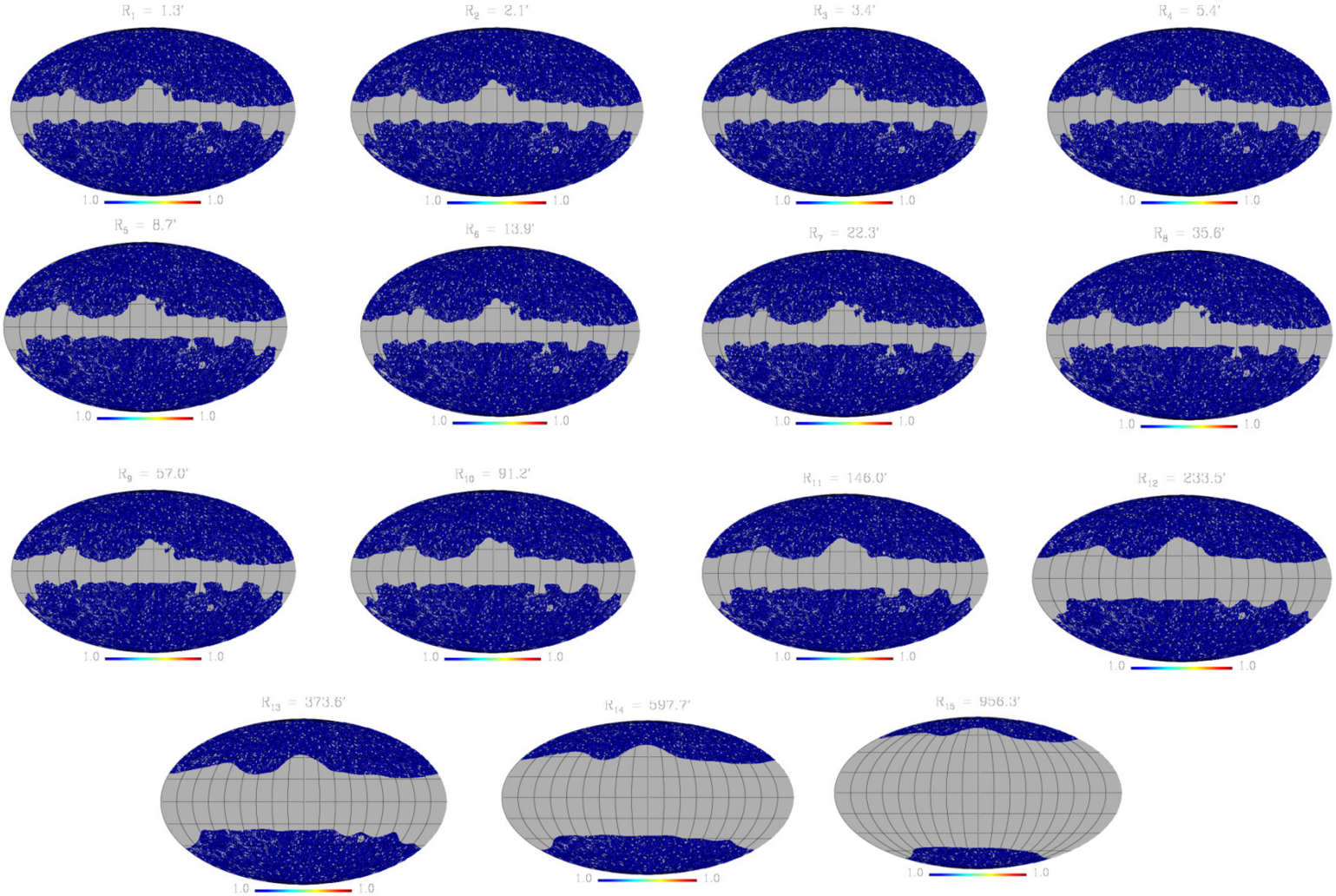

Generation of simulations of correlated noise

1. Compute the noise jackknife map:

$$\Delta T_{noise}(p) = \frac{\Delta T_{jackmap,A}(p) - \Delta T_{jackmap,B}(p)}{w(p)} \qquad w^2(p) = N_{hit}(p) \times \left(\frac{1}{N_{hit,A}(p)} + \frac{1}{N_{hit,B}(p)} \right)$$

2. Normalize the noise jackknife map by the noise RMS per pixel:

$$U_{noise}(p) = \frac{\Delta T_{noise}(p)}{\sigma_{noise}(p)}$$

3. Estimate the power spectrum of the normalized map: $C_\ell^{noise\ jk}$

4. Generate Gaussian simulations $\tilde{U}_{noise}(p)$ using the previous power spectrum.

5. Multiply the previous simulations by the noise RMS per pixel to introduce the anisotropies in the simulations:

$$\Delta \tilde{T}_{noise}(p) = \tilde{U}_{noise}(p) \times \sigma_{noise}(p)$$

Planck noise parameters

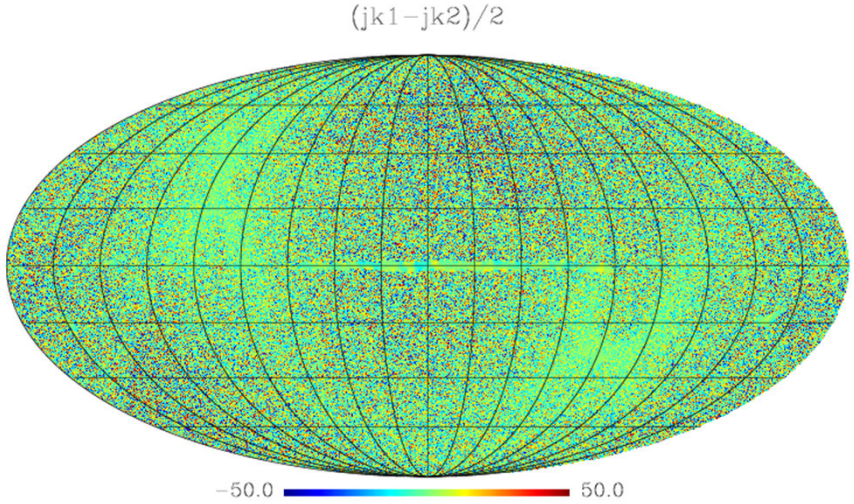

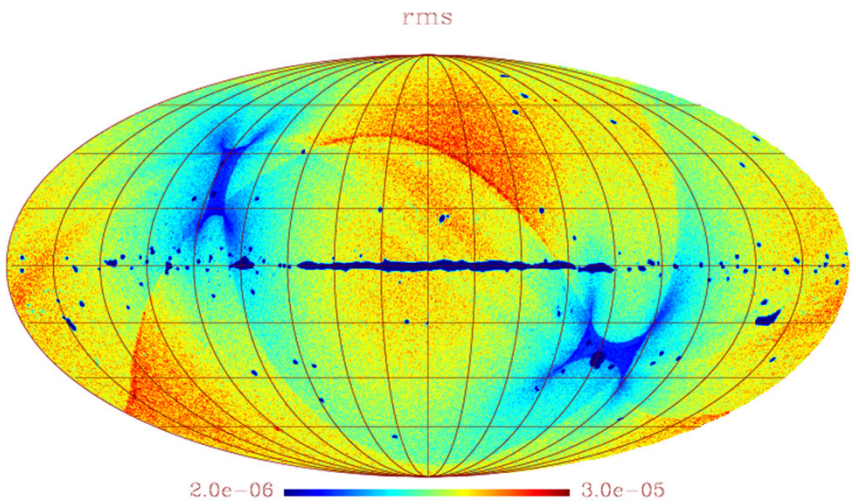

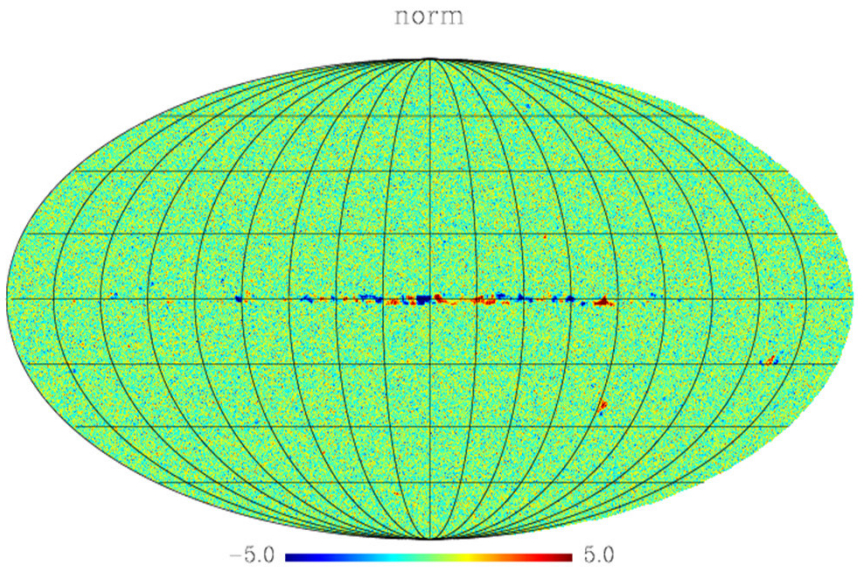

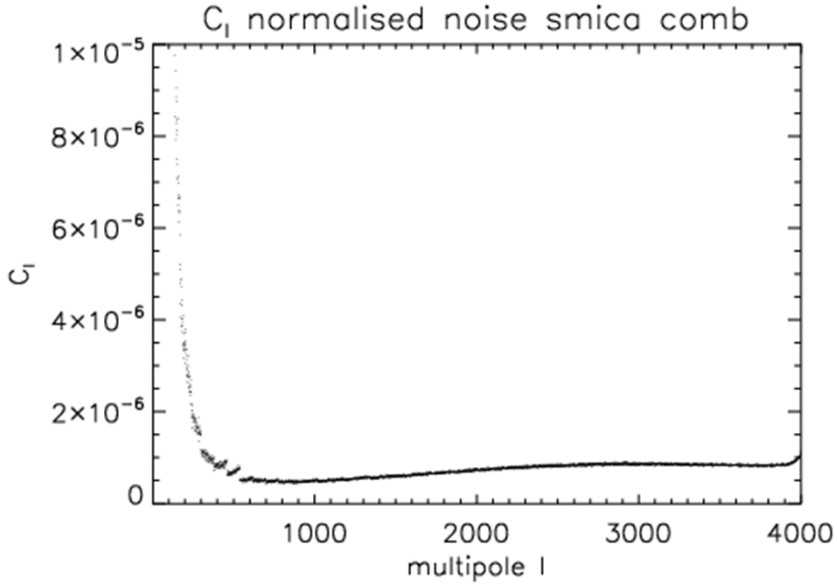

Two ways to estimate f_{nl}

Independent estimate for each shape:

$$\chi^2(f_{nl}) = \sum_{ijk,rst} (q_{ijk}^{data} - f_{nl}\alpha_{ijk}^{f_{nl}}) C_{ijk,rst}^{-1} (q_{rst}^{data} - f_{nl}\alpha_{rst}^{f_{nl}})$$

1) Minimization of the $\chi^2(f_{nl})$

Lensing subtraction and marginalization on the diffuse point source bispectrum:

$$\chi^2(f_{nl}, b_{ps}) = \sum_{ijk,rst} (q_{ijk}^{data} - \langle q_{ijk} \rangle_{ISWL} - b_{ps}\alpha_{ijk}^{ps} - f_{nl}\alpha_{ijk}^{f_{nl}}) C_{ijk,rst}^{-1} (q_{rst}^{data} - \langle q_{rst} \rangle_{ISWL} - b_{ps}\alpha_{rst}^{ps} - f_{nl}\alpha_{rst}^{f_{nl}})$$

1)Compute the likelihood $L(f_{nl}, b_{ps}) \propto \exp\left[-\chi^2(f_{nl}, b_{ps})/2\right]$

2)Sum on the PS bispectrum $P(f_{nl}) \equiv \sum_{b_{ps}} L(f_{nl}, b_{ps})$

3)Maximize P $P(f_{nl})$

Planck f_{nl} estimates using wavelets

Independent estimates

local

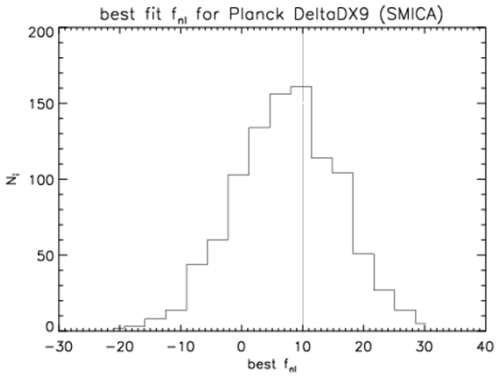

equilateral

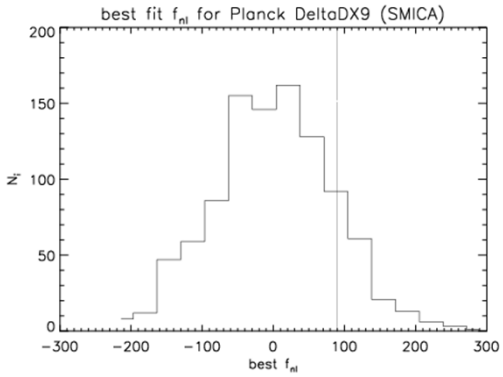

orthogonal

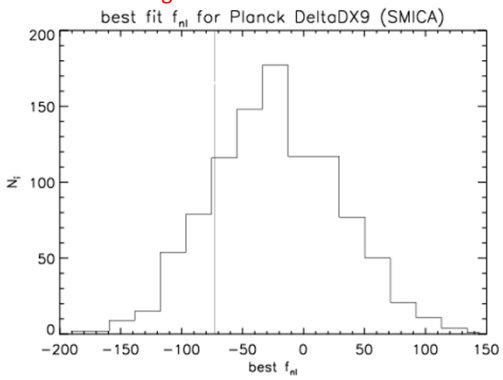

shape	Local	Equilateral	Orthogonal
f_{nl}	10	89	-73
$\sigma(f_{nl})$	8.5	84	52

Error-bars obtained with realistic Planck simulations with lensing NG signal

Planck f_{nl} estimates using wavelets

Subtraction of ISW-lensing amplitude and point source marginalization

local

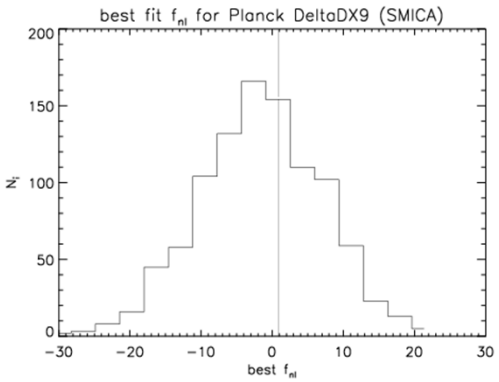

equilateral

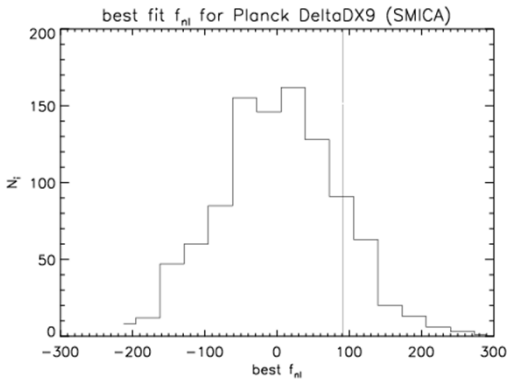

orthogonal

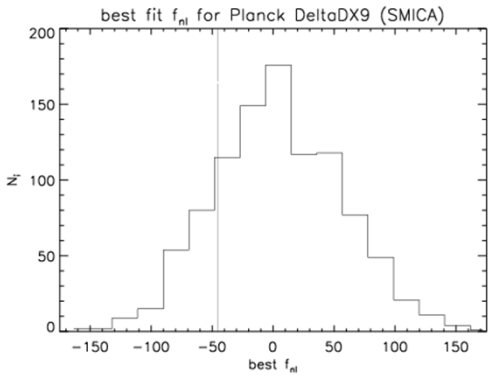

shape	Local	Equilateral	Orthogonal
f_{nl}	0.9	90	-45
$\sigma(f_{nl})$	8.5	84	52

Error-bars obtained with realistic Planck simulations with lensing NG signal

Table 9. Results for the f_{NL} parameters of the primordial local, equilateral, and orthogonal shapes, determined by the KSW, binned and modal estimators from the SMICA, NILC, SEVEM, and C-R foreground-cleaned maps. Both independent single-shape results and results marginalized over the point source bispectrum and with the ISW-lensing bias subtracted are reported; error bars are 68% CL.

	Independent			ISW-lensing subtracted		
	KSW	Binned	Modal	KSW	Binned	Modal
SMICA						
Local	9.8 ± 5.8	9.2 ± 5.9	8.3 ± 5.9	$\mathbf{2.7 \pm 5.8}$	2.2 ± 5.9	1.6 ± 6.0
Equilateral	-37 ± 75	-20 ± 73	-20 ± 77	$\mathbf{-42 \pm 75}$	-25 ± 73	-20 ± 77
Orthogonal	-46 ± 39	-39 ± 41	-36 ± 41	$\mathbf{-25 \pm 39}$	-17 ± 41	-14 ± 42
NILC						
Local	11.6 ± 5.8	10.5 ± 5.8	9.4 ± 5.9	4.5 ± 5.8	3.6 ± 5.8	2.7 ± 6.0
Equilateral	-41 ± 76	-31 ± 73	-20 ± 76	-48 ± 76	-38 ± 73	-20 ± 78
Orthogonal	-74 ± 40	-62 ± 41	-60 ± 40	-53 ± 40	-41 ± 41	-37 ± 43
SEVEM						
Local	10.5 ± 5.9	10.1 ± 6.2	9.4 ± 6.0	3.4 ± 5.9	3.2 ± 6.2	2.6 ± 6.0
Equilateral	-32 ± 76	-21 ± 73	-13 ± 77	-36 ± 76	-25 ± 73	-13 ± 78
Orthogonal	-34 ± 40	-30 ± 42	-24 ± 42	-14 ± 40	-9 ± 42	-2 ± 42
C-R						
Local	12.4 ± 6.0	11.3 ± 5.9	10.9 ± 5.9	6.4 ± 6.0	5.5 ± 5.9	5.1 ± 5.9
Equilateral	-60 ± 79	-52 ± 74	-33 ± 78	-62 ± 79	-55 ± 74	-32 ± 78
Orthogonal	-76 ± 42	-60 ± 42	-63 ± 42	-57 ± 42	-41 ± 42	-42 ± 42

Planck Collaboration XXIV

Table 2. Amplitudes $A^{T\phi}$, errors σ_A and significance levels of the non-Gaussianity due to the ISW effect, for all component separation algorithms (C-R, NILC, SEVEM, and SMICA) and all the estimators (potential reconstruction, KSW, binned, and modal). For the potential reconstruction case, an additional minimum variance (MV) map has been considered (see Planck Collaboration XVII 2013 for details).

Estimator		C-R		NILC		SEVEM		SMICA		MV	
$T\phi$	$\ell \geq 10$	0.52 ± 0.33	1.5	0.72 ± 0.30	2.4	0.58 ± 0.31	1.9	0.68 ± 0.30	2.3	0.78 ± 0.32	2.4
	$\ell \geq 2$	0.52 ± 0.32	1.6	0.75 ± 0.28	2.7	0.62 ± 0.29	2.1	0.70 ± 0.28	2.5		
KSW		0.75 ± 0.32	2.3	0.85 ± 0.32	2.7	0.68 ± 0.32	2.1	0.81 ± 0.31	2.6		
binned		0.80 ± 0.40	2.0	1.03 ± 0.37	2.8	0.83 ± 0.39	2.1	0.91 ± 0.37	2.5		
modal		0.68 ± 0.39	1.7	0.93 ± 0.37	2.5	0.60 ± 0.37	1.6	0.77 ± 0.37	2.1		

Planck Collaboration XIX

Table 15. Estimates of $f_{\rm NL}^{\rm local}$ obtained with MFs on *Planck* data. Foreground and secondary effects are evaluated in terms of $f_{\rm NL}^{\rm local}$. Results are for SMICA at $N_{\rm side} = 1024$ and $\ell_{\rm max} = 2000$.

	$f_{\rm NL}^{\rm local}$	Source	Corresponding $\Delta f_{\rm NL}^{\rm local}$
Raw map	19.1 ± 19.3		–
Lensing subtracted	8.5 ± 20.5	Lensing	+10.6
Lensing+PS subtracted	7.7 ± 20.3	Point sources	+0.8
Lensing+CIB subtracted	7.5 ± 20.5	CIB	+1.0
Lensing+SZ subtracted	6.0 ± 20.4	SZ	+2.5
All subtracted	4.2 ± 20.5	All	+14.9

Planck Collaboration XXIV

Summary

- Three particular NG shapes are considered to constrain the inflationary scenario
  - f_{nl} local
  - f_{nl} equilateral
  - f_{nl} orthogonal
- The f_{nl} shapes are given in terms of the CMB anisotropies
- Contaminants for WMAP and Planck frequencies:
  - Lensing
  - Point sources
- Estimator: wavelets
- Results
  - Detection of the ISW-lensing signal
  - Agreement with direct bispectrum-based estimators
  - Once the ISW-lensing signal is removed, the data are compatible with Gaussianity
- Next:
  - Point source bias
  - Optimality
  - Polarization